Shedding Plasma Membrane Vesicles Induced by Graphene Oxide Nanoflakes in Brain Cultured Astrocytes

note finali coverpage

(Article begins on next page)

17 May 2024

Journal Pre-proof

Shedding Plasma Membrane Vesicles Induced by Graphene Oxide Nanoflakes in Brain Cultured Astrocytes

Mattia Musto, Pietro Parisse, Maria Pachetti, Christian Memo, Giuseppe Di Mauro, Belen Ballesteros, Neus Lozano, Kostas Kostarelos, Loredana Casalis, Laura Ballerini

Please cite this article as: M. Musto, P. Parisse, M. Pachetti, C. Memo, G. Di Mauro, B. Ballesteros, N. Lozano, K. Kostarelos, L. Casalis, L. Ballerini, Shedding Plasma Membrane Vesicles Induced by Graphene Oxide Nanoflakes in Brain Cultured Astrocytes, *Carbon*, https://doi.org/10.1016/j.carbon.2021.01.142.

This is a PDF file of an article that has undergone enhancements after acceptance, such as the addition of a cover page and metadata, and formatting for readability, but it is not yet the definitive version of record. This version will undergo additional copyediting, typesetting and review before it is published in its final form, but we are providing this version to give early visibility of the article. Please note that, during the production process, errors may be discovered which could affect the content, and all legal disclaimers that apply to the journal pertain.

Shedding Plasma Membrane Vesicles Induced by Graphene Oxide Nanoflakes in Brain Cultured Astrocytes

Mattia Musto[1][†], Pietro Parisse[2], Maria Pachetti[2], Christian Memo[1], Giuseppe Di Mauro[1], Belen Ballesteros[3], Neus Lozano[3], Kostas Kostarelos[3,4], Loredana Casalis[2] and Laura Ballerini[1*]*

[1]International School for Advanced Studies (SISSA), 34136 Trieste, Italy

[2]ELETTRA Synchrotron Light Source, 34149 Basovizza, Italy

[3]Catalan Institute of Nanoscience and Nanotechnology (ICN2), Campus UAB, Bellaterra, 08193 Barcelona, Spain

[4]Nanomedicine Lab, National Graphene Institute and Faculty of Biology, Medicine & Health The University of Manchester, Manchester M13 9PT, United Kingdom

Graphene

Shedding Plasma Membrane Vesicles Induced by Graphene Oxide Nanoflakes in Brain Cultured Astrocytes

Mattia Musto[1][†], Pietro Parisse[2], Maria Pachetti[2], Christian Memo[1], Giuseppe Di Mauro[1], Belen Ballesteros[3], Neus Lozano[3], Kostas Kostarelos[3,4], Loredana Casalis[2][*] and Laura Ballerini[1][*]

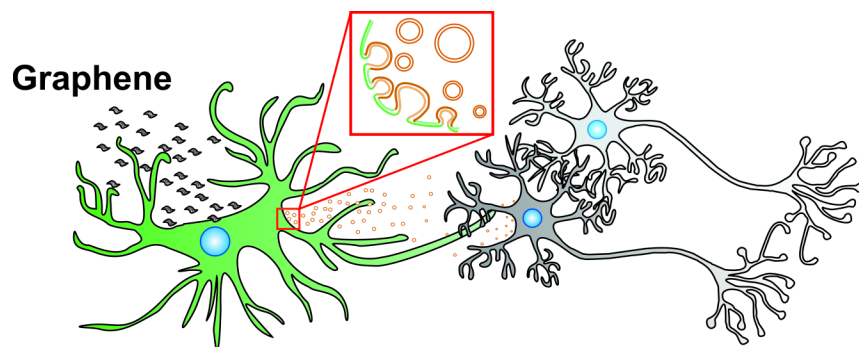[1]International School for Advanced Studies (SISSA), 34136 Trieste, Italy

[2]ELETTRA Synchrotron Light Source, 34149 Basovizza, Italy

[3]Catalan Institute of Nanoscience and Nanotechnology (ICN2), Campus UAB, Bellaterra, 08193 Barcelona, Spain

[4]Nanomedicine Lab, National Graphene Institute and Faculty of Biology, Medicine & Health The University of Manchester, Manchester M13 9PT, United Kingdom

Abstract

Microvesicles (MVs) generated and released by astrocytes, the brain prevalent cells, crucially contribute to intercellular communication, representing key vectorized systems able to spread and actively transfer signaling molecules from astrocytes to neurons, ultimately modulating target cell functions. The increasing clinical relevance of these signaling systems requires a deeper understanding of MV features, currently limited by both their nanoscale dimensions and the low rate of their constituent release. Hence, to investigate the features of such glial signals, nanotechnology-based approaches and the applications of unconventional, cost-effective tools in generating MVs are needed. Here, small graphene oxide (s-GO) nanoflakes are used to boost

22 MVs shedding from astrocytes in cultures and s-GO generated MVs are compared with those

23 generated by a natural stimulant, namely ATP, by atomic force microscopy, light scattering,

24 attenuated total reflection–fourier transform infra-red and ultraviolet resonance Raman

25 spectroscopy. We also report the ability of both types of MVs, upon acute and transient exposure

26 of patch clamped cultured neurons, to modulate basal synaptic transmission, inducing a stable

27 increase in synaptic activity accompanied by changes in neuronal plasma membrane elastic

28 features.

29

30 **Keywords:** graphene oxide, extracellular vesicles, atomic force microscopy and spectroscopy,

31 FTIR-ATR and UVRR spectroscopy, synaptic activity, cortical neuronal cultures

32

33 **1. Introduction**

34 In biology, newly described forms of intercellular communication comprise the release of

35 vesicles, named extracellular vesicles, from virtually all cell types, including resident glial cells

36 of the central nervous system (CNS), such as astrocytes and microglia.[1,2] In particular, the

37 shedding of membrane vesicles is a recognized form of cross talk in the multidimensional

38 signaling between astrocytes, (i.e. the majority of cells in the mammalian CNS), and neurons in

39 physiology, but also in neurodegenerative and neuroinflammatory diseases as well as in brain

40 tumors. Extracellular vesicle signaling molecules, either stored within their cargo or embedded in

41 their plasma membrane, modulate relevant processes in the development, physiology and

42 pathology of CNS target cells.[3–6] The signaling system based on release of extracellular

43 vesicles comprises shedding microvesicles (MVs) and exosomes, characterized by different size,

44 membrane composition, cargo and origin.[7,8]

45 MVs are nanovesicles able to interact specifically with cells at local or distant sites.[9] In

46 maintaining CNS functions, glial cells intensely communicate with neurons, also *via* the release

47 of MVs, which represents a highly versatile tool to functionally impact the CNS.[10–12] MVs

48 are considered a "vectorized" signaling system able to bind their target cells to transmit specific

49 information. The reported spreading ability of MVs has suggested their potential exploitation as

50 biomarkers or as engineered therapeutic carriers.[13] A comprehensive correlation between

51 conditions used to release and harvest MVs from the same cell type, i.e. astrocytes, and their

52 signaling ability, will impact our understanding of MVs physiology and the design of MV-based

53 biomedical applications in the CNS.[14,15] Particular attention has to be conveyed to devise

54 novel, cost-effective ways in generating MVs, in particular enhancing constitutive release.

55   Here, we concentrate on graphene oxide (GO), the most common derivative of graphene,

56 whose properties can be tailored to adapt to new physical and biological applications.[16,17] GO

57 flakes have been successfully designed for drug delivery applications in biomedicine.[18] In the

58 CNS, small GO nano-flakes (s-GO) were shown to induce constitutive MV release from cultured

59 astrocytes and to potentiate evoked MV release induced upon exposure to bzATP.[19] s-GO

60 flakes, due to their physical features at the nanoscale, were reported to interfere with cellular

61 membrane dynamics.[19,20] In addition, *via* adhesion to the plasma membrane, s-GO may alter

62 the mechanical features of the lipid bilayer[21] triggering genuine biological responses, such as

63 MVs signaling. Thus s-GOs may represent a tool to exploit mechanical signaling at the

64 nanoscale to activate membrane release of MVs. Drug delivery applications where vesicle

65 release from genetically engineered cells is required, may take advantage of the mechanical

66 modulation of vesicle release brought about by graphene-based nanomaterials, representing a

67 safer and cheaper alternative to pharmacological tools. Prolonged exposure to biomolecules able

3

68   to induce MVs release, such as ATP, could in fact negatively affect cell physiology by

69   promoting astrogliosis and inducing microglia-mediated neuroinflammatory responses.[22]

70   We use the ability of s-GO to substantially increase the production of MVs from astrocytes to

71   provide, for the first time, a robust and comparative vesicle characterization by means of ultra-

72   microscopy, attenuated total reflection–fourier transform infra-red (FTIR-ATR) and UV

73   Resonant Raman (UVRR) spectroscopy. We additionally explore by single cell patch-clamp

74   recordings the impact of acute, local and transient delivery of MVs on neuronal basal synaptic

75   activity and by atomic force microscopy (AFM) the accompanying changes in neuronal plasma

76   membrane elastic features.

77   **2. Material and Methods**

78   *2.1 Graphene oxide nanosheets synthesis*

79   GO was manufactured under endotoxin-free conditions through our modified Hummers' method

80   as previously described.[19] The complete characterization of the material used is shown and

81   summarised in the Supplementary experimental section and Supplementary Figure S1 and Table

82   S1.

83   *2.2 Cell Cultures*

84   All experiments were performed in accordance with the EU guidelines (Directive 2010/63/EU)

85   and Italian law (decree 26/14) and were approved by the local authority veterinary service and by

86   our institution (SISSA-ISAS) ethical committee. All efforts were made to minimize animal

87   suffering and to reduce the number of animals used. Animal use was approved by the Italian

88   Ministry of Health, in agreement with the EU Recommendation 2007/526/EC.

89   Primary glial cultures were obtained from cortices isolated from neonatal rats (Wistar) at

90   postnatal day 2-3 (P2–P3), as previously described [19,23]. Dissociated cells were plated into

4

91 plastic 150 cm^2 flasks and incubated at 37 °C; 5 % CO_2 in culture medium composed of DMEM

92 (Invitrogen), supplemented with 10 % fetal bovine serum (FBS; Thermo Fisher), 100 IU/ mL

93 penicillin, and 10 mg/mL streptomycin.

94 Cortical neurons were isolated from neonatal rat cortices (Wistar) at postnatal day 0-1

95 (P0–P1). Dissociated cells were then plated on poly-L-ornithine (Sigma) coated coverslips

96 (Kindler, EU) at a concentration of 150000 cells in a volume of 200 μL and incubated at 37 °C; 5

97 % CO_2 in a culture medium composed of Neurobasal-A (Thermo Fischer) containing 2% B27

98 (Gibco), 10 mM Glutamax and 0.5 μM Gentamycin (Gibco) for 8-10 *days in vitro* (DIV) before

99 performing electrophysiological experiments.

100 *2.3 MV Isolation*

101 MV shedding and isolation was performed as previously described.[19] One pool of MVs

102 were collected from 21-24 DIV glial cultures previously treated with graphene oxide nanoflakes

103 (s-GO) (10 μg/mL[19]), added to culture medium once and left for 6 days. At the end of 6-days

104 exposure, the medium was removed and substituted with physiological saline solution, with the

105 following composition: 152 mM NaCl, 4 mM KCl, 1 mM $MgCl_2$, 2 mM $CaCl_2$, 10 mM HEPES

106 and 10 mM Glucose (pH adjusted to 7.4), at 37 °C and 5 % CO_2 for 60 min prior to MVs

107 collection and purification. The MVs pool was isolated from cultures treated (30 min) with

108 benzoyl-ATP (bzATP; 100 μM) diluted in physiological saline solution. The 6-days exposure

109 timepoint was chosen on the basis of previous western blot experiments, and confirmed by our

110 current experiments testing MVs release after 3 days of s-GO exposure (supplementary Figure

111 S2).[19] Negative controls were incubated with physiological solution without the presence of

112 bzATP or s-GO. After the incubation period, cell medium was collected and centrifuged for 15

113 min at a speed of $300 \times g$ in order to remove cell debris. Supernatant was then collected and

114   MVs were pelleted by centrifugation at $20000 \times g$ for 2 hours. For Ca^{2+} deprivation experiments,

115   prior to supernatant collection and MVs pellet centrifugation, cultures were pre-incubated for 45

116   min in a saline solution identical to the physiological saline solution except for 0 mM $CaCl_2$, 3

117   mM $MgCl_2$ and 1mM EGTA to allow the depletion of intracellular calcium storage. Upon this

118   pre-treatment, we harvest the MVs from controls, s-GO treated and bzATP (30 min in Ca^{2+}

119   deprived solution; supplementary Figure S3).

120   *2.4 Western blot analysis*

121   MVs were prepared as previously reported, briefly they were re-suspended in lysis buffer (50

122   mM Tris-HCl, pH 8.0, 150 mM NaCl, 1 % NP40, 0.1 % SDS), sonicated for 30 s, and then

123   boiled at 95 °C for 5 min.[19] Samples were run on a 10 % polyacrylamide gel and blotted onto

124   nitrocellulose membranes (Millipore, Italy). Membranes were then blocked in PBS-Tween-20

125   (0.1 %) plus 5 % nonfat dry milk and incubated with the primary antibody antiflotillin-1 (dilution

126   1:1000) for 16 h at 4 °C. Membranes were then washed with PBS-Tween and incubated with

127   peroxidase-conjugated anti-mouse secondary antibody (dilution 1:1000). Detection of

128   immunolabeled ECL-exposed protein bands was measured with UVI-1D software over three

129   independent experiments.

130   *2.5 Immunofluorescence and confocal microscopy*

131   Primary glial and cortical neurons cultures were fixed in 4 % formaldehyde (PFA, prepared

132   from fresh paraformaldehyde) in PBS for 20 min at room temperature (RT) and then washed in

133   PBS. Free aldehyde groups were quenched in 0.1 M glycine solution for 5 min. The samples

134   were permeabilized in 5 % fetal bovine serum (FBS), 0.3 % Triton-X 100 in phosphate buffer

135   solution (PBS) for 30 min at RT. Samples were then incubated with primary antibodies (mouse

136   monoclonal anti-GFAP, Invitrogen, 1:500 dilution; rabbit polyclonal anti-β-tubulin III, Sigma-

6

137   Aldrich, 1:500 dilution) diluted in PBS with 5 % FBS at 4 °C for 1 hours. Samples were then

138   incubated with secondary antibodies (Alexa 488 goat anti-mouse, Invitrogen, 1:500 dilution;

139   Alexa 594 goat anti-rabbit, Invitrogen, 1:500 dilution), and DAPI (Invitrogen, dilution 1:200) to

140   stain the nuclei, for 45 min at RT and finally mounted on 1 mm thick glass coverslips using

141   Fluoromount mounting medium (Sigma-Andrich). Images were acquired using a Nikon C2

142   Confocal, equipped with Ar/Kr, He/Ne and UV lasers with a 40 $\times$ or 60 $\times$ (1.4 NA) oil-objective

143   (using oil mounting medium, 1.515 refractive index) to acquire glial cultures images and cortical

144   neurons images respectively. 200 $\times$ 200 µm fields were acquired for cortical neurons images and

145   300 $\times$ 300 µm fields were acquired for glial cells images. Confocal sections were acquired every

146   0.25 µm for both the cultures.

147   *2.6 Glial cell viability assay*

148   Primary rat astrocytes (21-24 DIV) were exposed to s-GO 10 μg/mL or to equivalent volumes

149   of the vehicle for 6 days. Cells were stained with propidium iodide (PI, 1 µg/ml; 15 min) for cell

150   death quantification and subsequently fixed in PFA and labelled for DAPI for nuclei

151   visualization and GFAP for visualizing astrocytes. The red (PI positive) fluorescent nuclei

152   indicating dead cells were quantified at 40 $\times$ (1.4 NA) magnification using a Nikon C2 Confocal

153   microscope, equipped with Ar/Kr, He/Ne and UV lasers, with random sampling of 10 fields per

154   sample (n = 3 coverslips/sample, from 3 independent culture preparations). The average

155   percentage of dead cells was calculated counting visual fields selected.

156   *2.7 FM1-43 staining*

157   Glial cells were incubated with the fluorescent styryl dye FM1-43 (2 μM) for 2 min in order to

158   completely stain plasma membrane, then extensively washed with PBS and exposed for 30 min

159   to bzATP (100 μM) or to standard saline solution.[19] Samples were placed in a recording

7

160 chamber mounted on an inverted microscope (Nikon Eclipse Ti-U) and observed with a 40 ×

161 objective (0.6 NA, PlanFluor, Nikon). Images (512 × 512 px) were acquired for 10 min with an

162 exposure time of 150 ms (6.6 Hz) by a Hamamatsu Orca-Flash 4.0 digital camera controlled by

163 an integrating imaging software package (HCImage, Hamamatsu). Recorded images were

164 analyzed offline with the Clampfit software (pClamp suite, 10.2 version; Axon Instruments).

165 Image time stacks were analyzed in selected regions of interest (ROI) to measure the

166 variations in FM1-43 fluorescence intensity over time. Natural sample bleaching over time,

167 due to prolonged light exposure, has the same time-course and intensity in all the three

168 groups, as previously described[19].

169 *2.8 Atomic Force Microscopy Analysis*

170 AFM characterization was performed as previously described.[19] Briefly, the pellet of MVs

171 was re-suspended in PBS solution after isolation from cell cultures and a 15 μL drop of sample

172 solution was placed and left to adsorb (30 min) onto a freshly peeled mica substrate. Vesicles

173 were then fixed with 1% formaldehyde for 1 h (RT) in order to prevent their collapse during

174 AFM acquisition. MVs were then washed with PBS and dried under a gentle stream of nitrogen.

175 AFM analysis was performed in air at RT, using the semicontact mode of a commercial

176 instrument (Solver Pro, NT-MDT, RU). Silicon tips (NSC36/CR-AU, MikroMash, USA) with a

177 typical force constant of 0.6 nN/nm and a resonance frequency of about 65 kHz were employed.

178 Topographic height and phase images were recorded at 512 × 512 pixels at a scan rate of 0.5 Hz.

179 Image processing was performed using Gwyddion freeware AFM analysis software, version

180 2.40. Diameter and height of each vesicle were evaluated from cross-line profiles, and results

181 were statistically analyzed using Prism (Graphpad software).

182 *2.9 Neuronal Stiffness*

183   9-10 DIV cortical neurons were exposed to MVs obtained by glial cultures treated with bzATP

184   or s-GO and neuronal rigidity was assessed with AFM, 24 hours after MVs exposure. Force

185   spectroscopy measurements were performed with a commercial Smena AFM (NT-MDT, RU)

186   mounted on an inverted microscope (Nikon Eclipse Ti-U). AFM cantilever deflection was

187   measured when pushed against cortical neurons plated on a glass coverslip. Deflection values

188   were subsequently converted into a force versus indentation curve based on cantilever spring

189   constant and its displacement. Neuronal rigidity was evaluated in 50 randomly chosen neurons

190   for each condition (from 3 independent experiments), acquiring three force spectroscopy curves

191   in the center of each cell soma. The AFM tip was positioned by using an inverted microscope in

192   bright field mode.

193   AFM micro-cantilevers with an elastic constant of about 0.03 nN/nm and a resonance

194   frequency of about 10 kHz (CSG01 tipless cantilevers from NT-MDT, RU) were used. A

195   borosilicate glass microsphere of about 18 μm in diameter (18.2 ± 1.0 mm from Duke Standards,

196   CA, USA) was manually glued at the end of each cantilevers using a UV curable glue (Norland

197   Optical Adhesive 61 from Norland Products Inc., NJ, USA). Force spectroscopy measurements

198   were performed at a constant indentation speed of 1 mm/s with a maximum value of indentation

199   deepness set at 500 nm. Elastic modulus values (E), expressed in kPa, were determined by fitting

200   obtained force–indentation curves with a Hertzian model for the tip, using AtomicJ (v. 1.7.3)

201   analysis software.[24]

202   *2.10 Nanoparticle Tracking analysis (NTA)*

203   Measurement and analysis of MVs size distribution by NTA was performed on a NanoSight

204   LM10 system (Malvern) using approximately 500 μL of MVs of both conditions (bzATP-

205   derived and s-GO-derived) diluited 1:20 in MilliQ H_2O. Individual videos of 60 seconds

9

206 (recorded at 25 FPS; 3 videos per group) for each sample were acquired at RT using the

207 maximum camera gain, a detector threshold equal to 8 and analyzed by the NanoSight particle

208 tracking software to calculate size and vesicle concentration.

209 *2.11 FTIR-ATR Spectroscopy and UV Resonant Raman (UVRR) Measurements*

210 MVs were isolated from 21-24 DIV glial cultures by centrifugation as described above. MVs

211 pellet was successively washed with NaCl solution (150 mM) and finally re-suspended in 50 μL

212 of the same solution in order to avoid contribution of phosphate and sugar groups to the IR

213 absorbance spectra. The IR measurements were carried out at the BL10.2-IUVS beamline at

214 Elettra synchrotron Trieste. The spectra were collected in ATR mode using a MIR DLaTGS

215 detector and a KBr-broadband beam-splitter. For each IR measurement, 2 μL of sample solution

216 were spread over the whole area of a monolithic diamond ATR plate and left to dry forming a

217 thin film. For each sample, 20 spectra were collected in the range 4000-800 cm^{-1}, accumulating

218 256 scans for each spectrum reaching a resolution of 4 cm^{-1}. Each spectrum was corrected for the

219 background, aqueous vapor, CO_2 and not normalized to any absorbance band.

220 UVRR measurements were performed at the BL10.2-IUVS beamline at Elettra synchrotron

221 Trieste using the experimental set-up reported.[25] 5 μL of vesicles solution were drop-casted

222 onto an aluminum foil, allowed to dry and kept under nitrogen purging. All the measurements

223 were performed at RT, using an excitation wavelength of 244 nm and tuning the power of the

224 incoming radiation to 50 μW. The outcoming radiation was collected in backscattering geometry

225 by using a triple stage spectrometer (Trivista, Princeton Instrument) with a spectral resolution of

226 8 cm^{-1}. Samples were continuously oscillated horizontally in order to avoid photodamaging.

227 *2.12 Electrophysiological Recordings*

228 Patch-clamp recordings (whole-cell, voltage clamp mode) were performed from visually

229 identified (under differential interference contrast - DIC - microscopy) cortical neurons (DIV 8-

230 10) placed in a recording chamber, mounted on an inverted microscope (Eclipse Ti-U, Nikon,

231 Japan) and superfused with control physiological saline solution of the following composition (in

232 mM): 152 NaCl, 4 KCl, 1 MgCl2, 2 CaCl2, 10 HEPES and 10 Glucose (pH adjusted to 7.4 by

233 NaOH 1M; osmolarity 300 mOsm). Cells were patched with glass pipettes (4-7 MΩ) containing

234 (in mM): 120 K gluconate, 20 KCl, 10 HEPES, 10 EGTA, 2 $MgCl_2$ and 2 Na_2ATP (pH adjusted

235 to 7.35 by KOH; osmolarity 298 mOsm). All electrophysiological recordings were performed at

236 RT and the spontaneous, basal synaptic activity was recorded by clamping the membrane voltage

237 at –70 mV (corrected for liquid junction potential, which was –14 mV). To investigate the acute

238 effect on synaptic activity of glia-derived MVs, an injection pipette (patch pipette with resistance

239 of 1–4 MΩ) filled with MVs previously isolated glial cultures as described above and re-

240 suspended in 100 μL of extracellular saline solution was positioned at 200 μm from the cell soma

241 and connected to a pico-spritzer (PDES-02DX, npi Electronics) with 0.3 psi in-line pressure.[19]

242 On the basis of MVs quantification obtained by NTA measurements, and considering that MVs

243 isolation was performed using the same protocol in all the experiments described, we calculated

244 that the concentration of MVs used for these tests was approximately of 6.64×10^9 for MVs

245 obtained by bzATP stimulation and 1.64×10^{10} for MVs isolated from s-GO treated cultures.

246 Baseline spontaneous synaptic activity was recorded for the 10 min prior delivering the puff

247 (500 ms duration) of MVs and followed up for 20 min to verify changes in post synaptic current

248 (PSC) frequency and amplitude induced by the fusion of MVs with neuronal membranes.

249 Data were collected by Multiclamp 700B patch amplifier (Axon CNS, Molecular Devices) and

250 digitized at 10 kHz with the pClamp 10.2 software (Molecular Devices LLC, USA). All

11

251 recorded events were analyzed offline with the AxoGraph 1.4.4 (Axon Instrument) event

252 detection software (Axon CNS, Molecular Devices).

253 *2.13 Statistical Analysis*

254   Data sets found to follow a non-normal distribution, were represented as box plot. The central

255 thick horizontal bar in the box plots indicates the median value, while the boxed area extends

256 from the 25th to 75th percentiles with the whiskers ranging from the 2.5[th] to the 97.5[th] percentiles.

257 Statistically significant differences between two non-parametric data sets were assessed by

258 Mann-Whitney's test, while to assess statistically significant differences among three data-set we

259 used the Kruskal-Wallis test and Dunn's post hoc test. $P < 0.05$ was considered at a statistically

260 significant.

261

262 **3. Results and discussion**

263 Astrocytes were isolated from postnatal (2-3 days) rat (Wistar) cortices, as previously

264 described.[19,20,23] We used visually homogenous s-GO dispersions containing s-GO

265 nanosheets with lateral dimensions predominantly between 50 – 500 nm.[19,20] We treated pure

266 glial cell cultures with s-GO (10 μg/mL) for 6 days.[19] Immunofluorescence labeling by antigen

267 against glial-fibrillary acidic protein (GFAP), an intermediate filament protein that is highly

268 specific for cells of the astroglial lineage, was used to visualize control and s-GO-treated

269 neuroglial cultures (GFAP, in green; Fig. 1a).[26] At the low concentrations used, s-GO

270 treatment did not impair astrocyte morphology and cell density when compared with matched

271 control cultures (box-plot in Fig. 1b).[19,27] Viability of glial cells was confirmed by propidium

272 iodide (PI) cell death assay. Control and s-GO treated cultures were incubated with PI, which

273 stain dead cells nuclei (Figure 1c, in red) and the percentage of PI-positive nuclei was calculated

274 (bar plot in Fig. 1d). Graphene nanosheets cytotoxicity is a largely debated issue, due to the

275 variable impact on cell toxicity of several material's features, related either on the GO physical-

276 chemical properties (thickness, size, surface functionalization, aggregation state and

277 concentration) or on the synthesis method[28,29], the experimental conditions adopted here and

278 in our previous works[19,20] exclude any cytotoxic effect on glial cells or neurons, both *in vitro*

279 and *in vivo*.

280   MVs are released into the extracellular space by direct budding from the plasma membrane of

281 astrocytes.[30] To explore the dynamics of MVs release in control, in s-GO treated and in ATP

282 treated (see below) astrocytes, we measured the presence of changes in membrane trafficking by

283 briefly incubating cultures with the fluorescent styryl dye FM1-43 and then quantifying the

284 astrocyte-membrane fluorescence decay to provide a cumulative measure of exocytosis in the

285 different growth conditions.[19,30]

286   FM dyes are fluorescent probes that reversibly stain membranes, and are largely used for

287 optical real-time measurements of membrane dynamics and secretory processes.[31–33]

288 Incubation with the FM dye (2 μM, 2 min) resulted in clear surface membrane staining of

289 control, bzATP, an agent known to evoke massive MVs release (100 μM, 30 min) and s-GO

290 treated cultures (10 μg/mL, 6 days), highlighted in Figure 1e (left panels).[30] Brighter spots

291 were considered as adherent debris and were excluded from the analysis. Besides these, both

292 bright and weak FM-stained plasma membrane domains were present along the whole

293 cytoplasmic surface and became visible within 2 min incubation (Fig. 1e). Due to this initial

294 variability in the intensity of the membrane staining, all FM de-staining measures were

295 normalized to the relative time 0. Once astrocyte membranes were labeled by the fluorescent dye

296 FM1-43 we measured the plasma membrane de-staining over a fixed time (10 min) in control, in

297 s-GO treated cultures, or during acute exposure to bzATP, under the same culturing

298 conditions.[19] Representative fluorescence intensity traces are shown in Figure 1f (top plot); the

299 dynamic of the fluorescence decay observed in control cultures, indicates the presence of

300 physiological bleaching of fluorophore over the acquisition time course, however s-GO and

301 bzATP groups, despite the same bleaching-induced loss of fluorescence, showed a faster de-

302 staining rate in respect to controls. This is also visualized by the time-lapse images framed at

303 time 0 s, 300 s and 600 s of the crude recordings (Figure 1e middle and right panels). We

304 quantified the fluorescence decay time constant (τ) values (box plot of Figure 1f) and detected

305 shorter decay values in both bzATP and s-GO groups (median$_{control}$= 219 s; median$_{bzATP}$= 184.2

306 s; median$_{s-GO}$= 163.9 s). This result suggested that the membrane de-staining was actually related

307 to MVs release, as expected in bzATP treated cells, more than to other membrane turnover

308 activities. Such a release was comparable between bzATP and s-GO, both significantly faster

309 than controls ($P_{bzATP} < 0.001$; $P_{s-GO} < 0.001$).

310

15
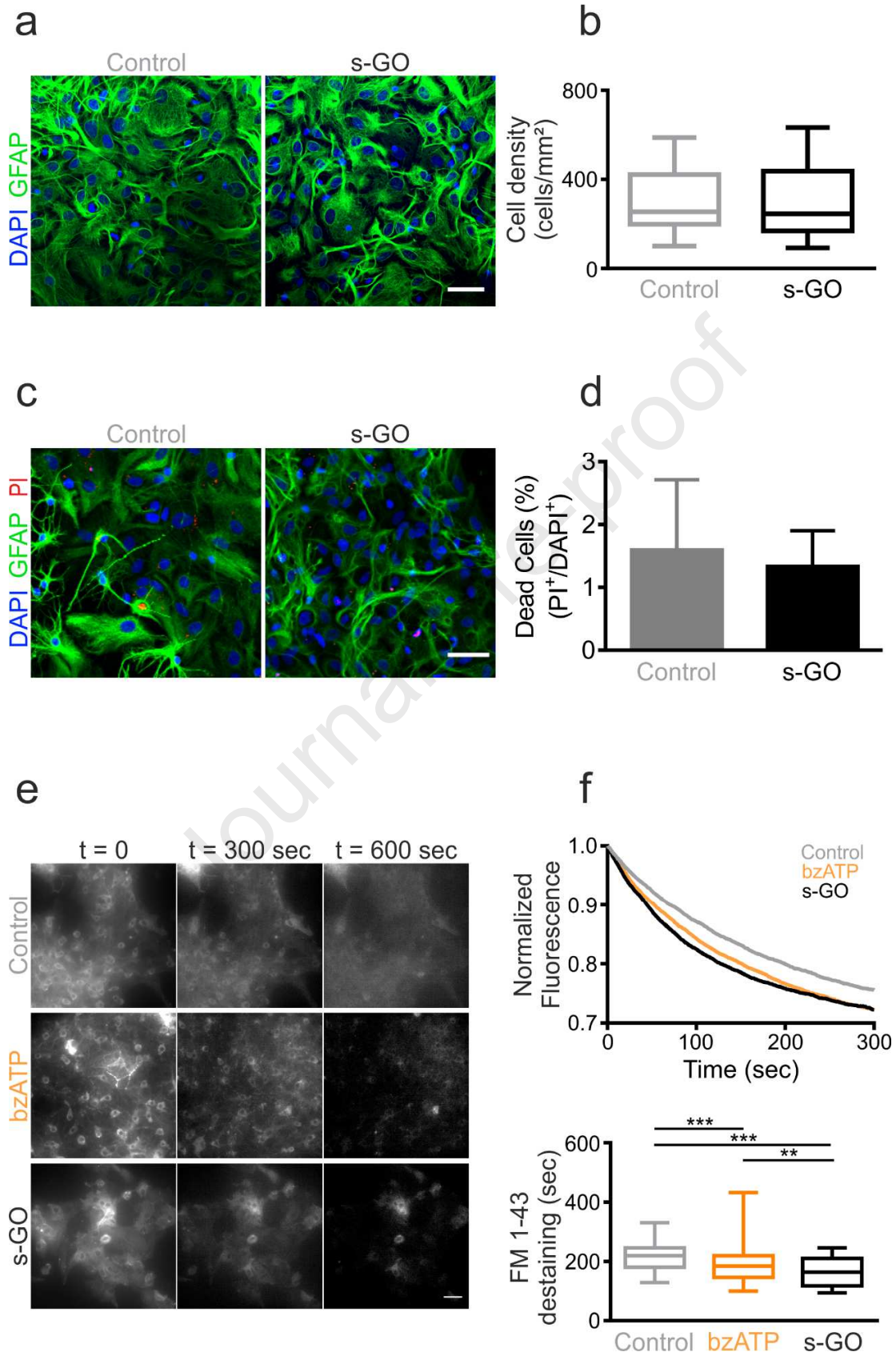
311   **Fig. 1. Graphene oxide nanosheets does not affect astrocytes vitality.** Cultured astrocytes release microvesicles
312   (MVs) upon ATP or s-GO stimulation. a) Confocal images visualize cultured astrocytes in control and after s-GO
313   (10 μg/mL; 6 days) treatment; anti-GFAP, in green, and DAPI (to visualize nuclei), in blue; scale bar 50 μm. b) Box
314   plot summarizes the cell density measures; note the similar values in both groups. c) Confocal images visualize
315   cultured astrocytes in control and after s-GO (10 μg/mL; 6 days) treatment. Cultures were treated with propidium
316   iodide (PI) to visualize death cells. Anti-GFAP, in green, DAPI (to visualize nuclei), in blue and PI in red; scale bar
317   50 μm. d) Histogram summarizes the percentage of death cells followed the s-GO exposure and in control condition;
318   note that there are no significant difference between two groups e) Surface membrane staining and activity
319   dependent de-staining of FM1-43 in cultured astrocytes, scale bar 25 μm. f) Normalized FM1-43 de-staining traces
320   (top) in control astrocytes (light grey), in bzATP treated once (orange) and in s-GO treated once (black). The box
321   plot (bottom) summarizes the decay time constant τ of FM1-43 de-staining in the three conditions ($median_{control}$ =
322   219.2 s; $median_{bzATP}$ = 184.2 s; $median_{s\text{-}GO}$ = 163.9 s). Thick horizontal bars in the box plots indicate median value;
323   boxed area extends from the 25th to 75th percentiles, whiskers from 2.5^{th} to the 97.5^{th} percentiles. Significance: **P <
324   0.01 ***P < 0.001, Kruskal-Wallis test, Dunn's post hoc test).

325

326   The release of MVs suggested by FM1-43 measures, was confirmed by immunoblot analysis

327   for the biomarker flotillin-1 of the supernatant collected from control and treated cultures (Fig.

328   2a). As expected, bzATP stimulation and s-GO incubation induced the appearance of a thick

329   band corresponding to flotillin-1 (Figure 2a), a signature of MVs release by astrocytes, with an

330   additive effect between s-GO exposure and pharmacological stimulation with bzATP ($s\text{-}GO_{Ringer}$

331   is quantified as 100 % more than $Control_{Ringer}$; $bzATP_{Ringer}$ is quantified as 360 % more than

332    $Control_{Ringer}$; $bzATP_{s\text{-}GO}$ is quantified as 2900 % more than $Control_{Ringer}$. Calculated over three

333   independent experiments).[19,30,34] In control conditions only a weak band was perceived,

334   indicating that MVs constitutive release in culture was poorly detectable. Atomic force

335   microscopy (AFM) topographic reconstruction of re-suspended MVs pellet (Fig. 2b) confirmed

336   the presence of MVs detected by the immunoblot in both bzATP (mvA) and s-GO (mvG)

337   groups. When investigating the effect of shorter (3 days) exposure to s-GO, western blot

338   experiments (supplementary Fig. S2) showed the absence of a significant increase in MVs

339   constitutive release when compared to control. Yet, bzATP release of MVs was potentiated by 3

340   days s-GO (supplementary Fig. S2) suggesting that s-GO already modulated MVs release, but

341   longer time of s-GO exposure are needed to enhance basal release in the absence of additional

342   stimuli. In an additional set of western blot experiments, we tested the sensitivity of bzATP and

343   s-GO MVs release to extracellular calcium deprivation (supplementary Fig. S3). Differently

344   from bzATP, s-GO release was apparently not affected by calcium removal. In control condition,

345   a thick band appeared upon calcium removal, suggestive of an increase in constitutive release

346   (supplementary Fig. S3). These preliminary results hint at release mechanisms differently tuned

347   by calcium among control, bzATP and s-GO and require further studies.

348   We systematically investigated and compared the MV size distribution by means of AFM and

349   nanoparticle tracking analysis (NTA) measurements. AFM images show the presence of

350   roundish protrusions of dimensions compatible with the size of MVs. No other kind of

351   contaminant was present, to indicate that the procedure for isolating and collecting MVs from the

352   medium was clean and effective. When analyzed by AFM (Fig. 2c) s-GO-derived MVs (mvG)

353   lateral size were significantly smaller (n = 72, median$_{mvG}$= 244 nm) than bzATP-derived ones

354   (mvA; n = 107, median$_{mvA}$= 479 nm) (P < 0.001). Conversely, we detected no differences in MV

355   height values (median$_{mvG}$= 19 nm; median$_{mvA}$= 22 nm; P = 0.17). Within each group, the

356   distribution of size values detected was not negatively correlated to the height, as shown in

357   Figure 2d (left; r$_{mvG}$= 0.8808 and r$_{mvA}$= 0.4039; P < 0.001). However, AFM experiments were

358   performed in air, thus a not specific flattening of MVs caused by vesicle collapsing might have

359   influenced these measurements. In principle differences in MV elastic properties, potentially

360   related to diverse membrane components, might lead to a variable collapsing of MVs when

361   measured in air.

362　　　Since AFM measurements are affected by the reduced size of the analyzed samples, and might

363　　not reflect the entire MVs population, we decided to use nanoparticle tracking analysis (NTA) to

364　　perform bulk analysis of vesicles in aqueous suspension. NTA tracks single particle Brownian

365　　motion within a dark field microscope, derives mean square vesicles velocity and translates them

366　　into size distribution.[35] NTA revealed a more complex pattern of size distribution (Fig. 2e): in

367　　the case of mvA we observed three subpopulations of vesicles at 115 nm, 235 nm and 400 nm

368　　respectively while in the case of mvG we found two partially overlapping peaks at 135 nm and

369　　168 nm, plus two distinct peaks at 275 nm and 385 nm (Fig. 2e). The diameter analysis revealed

370　　a slight, but not significant, difference between the two populations with the diameter of mvG

371　　smaller and less distributed, compared to those of mvA (median$_{mvA}$ = 235.4 nm; median$_{mvG}$ =

372　　183.6 nm) (Fig. 2f). These results convincingly suggested a comparable size distribution in both

373　　MV populations and subpopulations. However, we detected a significant difference in the

374　　number of vesicles released within the same time window (Fig. 2e) to indicate that cultures

375　　treated with s-GO produced more MVs when compared to cultures stimulated with bzATP (mvA

376　　=~3.32×10^8 vesicle/mL; mvG = ~8.19×10^8 vesicles/mL), consistently with our results obtained

377　　by MV release analysis and immunoblot (but see also Visnovitz et al. 2019[36]). Therefore, even

378　　though the overall size of the MV population produced did not change, s-GO was more efficient

379　　in generating MVs from astrocytes.

380
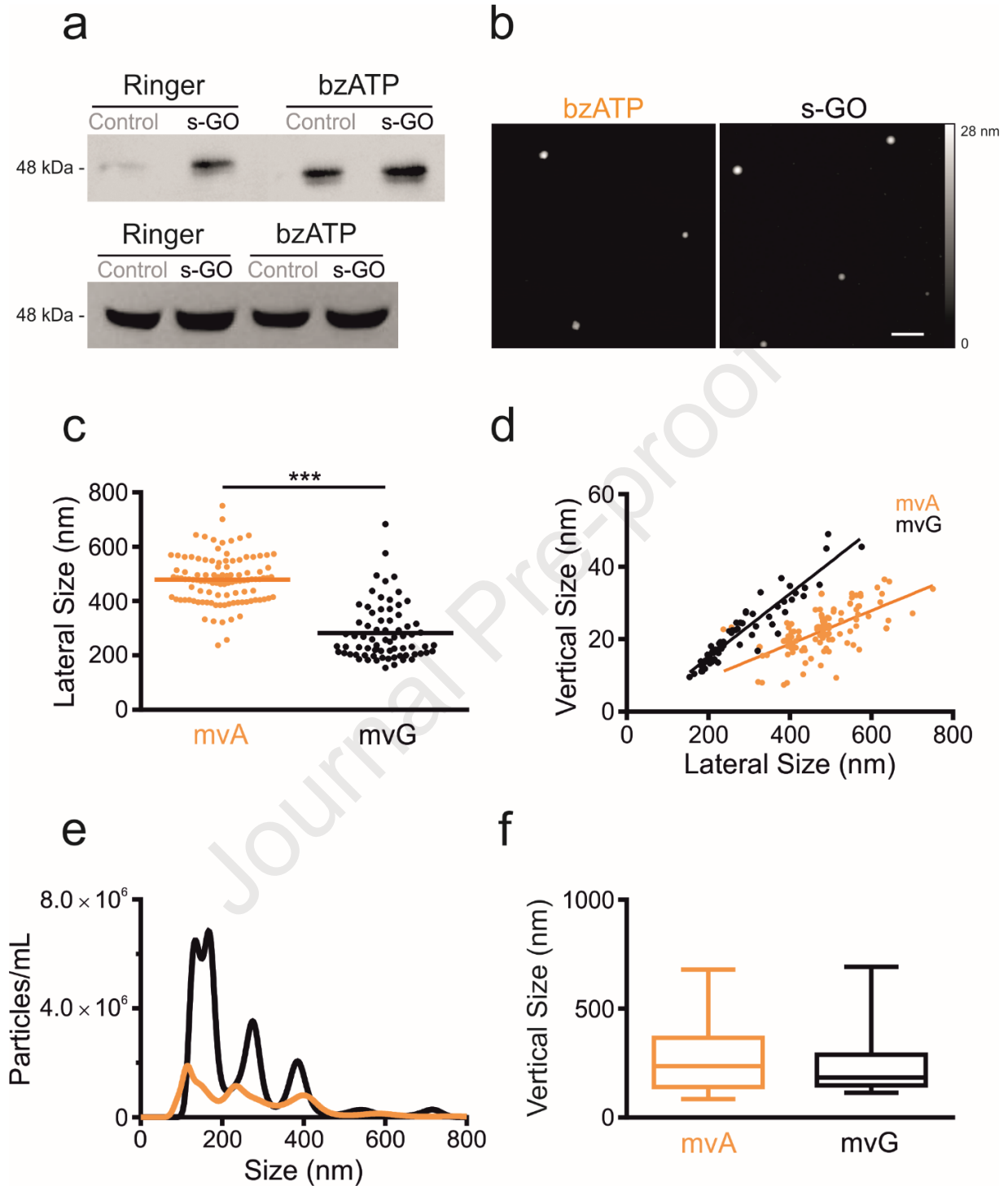
Fig. 2. Graphene oxide nanosheets and bzATP induce MVs release in Astrocytes. Microvesicle released by glial
cells *via* bzATP or s-GO stimulations characterized by ultra-resolution approaches**.** a) Western blotting of the pellets
(top row) and cell lysates (bottom row) for the MV marker flotillin-1 (N=3). Pellets were obtained from the medium
of glial cultures treated or untreated (control) with s-GO under two different conditions: not stimulated (ringer) or

385 stimulated (bzATP) by 100 μM bzATP. s-GO$_{Ringer}$ is quantified as 100% more than Control$_{Ringer}$; bzATP$_{Ringer}$ is

386 quantified as 360% more than Control$_{Ringer}$; bzATP$_{s-GO}$ is quantified as 2900% more than Control$_{Ringer}$. Calculated

387 over three independent experiments. b) AFM topographic reconstruction of MVs isolated from cultured primary

388 astrocytes treated with bzATP (100 μM) and s-GO (10 μg/mL) and performed in air (semi-contact mode). Scale bar

389 500 nm. c) Lateral size values distribution and median values for both groups, note that mvG lateral size is

390 significantly smaller than that of mvA (median$_{mvA}$ = 479 nm; median$_{mvA}$ = 244.1 nm; ***P > 0.001, Mann-Whitney

391 test). d) AFM measures of lateral size are plotted against AFM measures of height of MVs isolated from glial cells

392 treated by bzATP (100 μM; mvA; in orange) or by s-GO (10μg/mL; mvG; in black). e) Size distribution of MVs

393 isolated from glial cells treated by bzATP (100 μM; in orange) or by s-GO (10 μg/mL; in black) measured by

394 nanoparticle tracking analysis (NTA). Values of the peaks are expressed in nm. f) Lateral size values distribution

395 and median values for both groups, obtained by NTA measurement.

396

397

398   In order to analyze the macromolecular composition of MVs we took advantage of two

399 complementary techniques: FTIR-ATR and UVRR spectroscopy. For these measurements, MVs

400 were isolated by differential centrifugation as described before (see Material and Methods). To

401 avoid any spurious effect due to the absorption of phosphate groups from the buffer, we washed

402 and re-suspended the MVs pellet with a NaCl solution (150 mM). The infrared (IR) absorbance

403 spectra (Fig. 3a) revealed a clear contribution of the CH and the phosphate bands linked to DNA

404 in both samples, mvA and mvG, as well as the lipid signatures at 2900-3000 cm^{-1}, arisen from

405 the CH$_2$ and CH$_3$ stretching mode. The amide I and amide II bands between 1500 and 1785 cm^{-1},

406 the two major protein bands in the IR spectrum, show more pronounced differences between the

407 two populations of vesicles. The amide I band, which is primarily related to the C=O stretching

408 in the peptide bonds and modulated by the proteins' secondary structures, displayed similar

409 shapes for mvA and mvG. The amide II band, primarily due to C-N stretching and N-H in plane

410 bending vibrations, also reflecting the protein secondary structure, was instead clearly depleted

411 in the case of mvG. To gain insights into the contribution of different protein secondary

412 structures in the two families of vesicles, we analyzed the second derivative of the IR signal in

413 the amide I + amide II region (Fig. 3b) and used the position of the minima to guide a

414 multicomponent gaussian fit of the bands in the region 1500 and 1785 cm^{-1}. The % area

415 contributions obtained by the fit are reported in Fig. 3c. The low-energy flank of amide I of both

416 mvA and mvG is characterized by the presence of the 1610-1613 cm^{-1} vibrational peak which

417 could be addressed to a mixed contribution arisen from β-sheets and side-chains vibrations.

418 Additionally, the band at 1660 cm^{-1} might also be derived from the presence of RNA in the

419 vesicles.[37] Noteworthy, the relative populations of the peaks at approximately 1645 cm^{-1},

420 1660 cm^{-1} and 1678 cm^{-1} are inverted between mvA and mvG. According to the literature[37],

421 the 1645 cm^{-1} peak (depleted in mvG) might be assigned to random structures and/or helices; the

422 1660 cm^{-1} peak (depleted in mvA) to flexible helices (as 3_{10} helices); the 1678 cm^{-1} peak

423 (depleted in mvG) to beta structures such as b-turns. The bands at 1632 cm^{-1} and at 1693 cm^{-1},

424 both present in the mvG only, are ascribed to anti-parallel beta sheet, as found in aggregates in

425 tissues.[37,38] We can conclude that mvGs contain proteins with perturbed secondary structure,

426 characterized by beta structure-based aggregates and flexible helices. No significant variations in

427 the DNA phosphate bands were measured as well as the nature or localization of the DNA

428 signature detected. It is interesting to note that in previous measures the DNA delivered by EVs

429 has been reported to be stocked either inside the vesicles or on their surface[39].

430   UV Resonant Raman (UVRR) measurements taken using an excitation wavelength of 244 nm

431 (see experimental section and supplementary Fig. S4) confirmed the amide I signal depression in

432 mvG absorption spectrum. Due to an overlap between the UVRR s-GO band, we could not

433 confirm or discard the presence of s-GO inside the vesicles. Thus, we cannot exclude that the

434 changes in protein native structure might be due to s-GO altering the MV

435 micro(nano)environment or the possibility of a general interference with the measurements. The

436   absence of astrocytes cytotoxicity, even upon prolonged exposure to s-GO, together with the

437   functional measures of increased MVs release kinetic obtained by live imaging, are against a

438   mere alteration in protein integrity due to denaturation of membrane proteins in the presence of

439   s-GO.[40–42] FTIR-ATR spectroscopy is a powerful tool to assess the disordered character of

440   proteins, and the absence of a well-defined structure under native conditions is a peculiar

441   property of intrinsically disordered proteins (IDP).[43,44] In this framework, IDPs might

442   represent a specific signal vehiculated by mvG and the lack of protein structural constraints

443   could facilitate several, yet unknown, biological processes.[44]

a

b

c

444
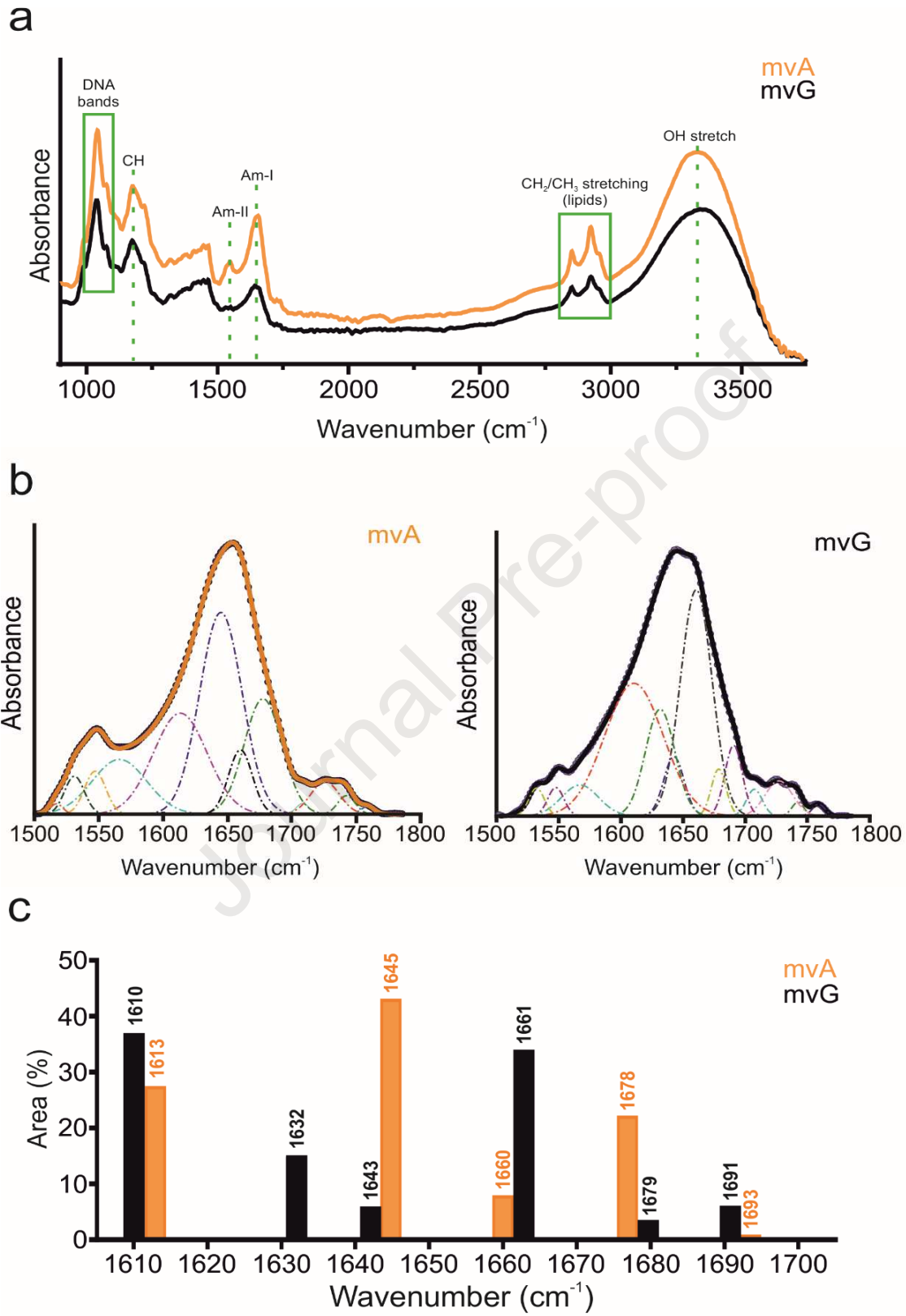
445 **Fig. 3. MVs characterization by infrared spectroscopy.** Microvesicles produced by glial cells *via* bzATP or s-GO

446 stimulation and characterized by infrared spectroscopy. a) Infrared spectra of microvesicles obtained by bzATP

447 stimulation (mvA, in orange) or by s-GO exposure (mvG, in black) in the region 950-3600 cm^{-1}. Contributions

448 arisen from nucleic acids, proteins and lipids characterize the spectra. The two boxes in green and the green dashed

449 lines are used as eye-guides to highlight nucleic acids, CH_2-CH_3 stretching of lipids and protein amide bands,

450 respectively. b) Fitting procedure applied to mvA (on the left) and mvG (on the right) amide bands spectra.

451 Multicomponent Gaussian curves were used to actually reproduce the experimental data. The centres of the

452 Gaussian curves were chosen as the minimum of the 2nd derivative of the spectrum and kept free to variate within 4

453 cm^{-1} around its maximum. c) Histograms representing the areas of the Gaussian curves used to reproduce the

454 experimental data of mvA (in orange) and mvG (in black) in the region 1500-1785 cm^{-1}. The areas of each band has

455 been weighted respect to the total amide band area which they belongs to (i.e. 1640 cm^{-1} band has been weighted

456 with respect to the total Am-I band area).

457 It is clearly visible that mvA and mvG vesicles have a different secondary structure: the former is mainly

458 characterized by an intense peak at 1645 cm^{-1} (43%), which can be assigned to random structures/a-helix structure,

459 and at 1678 cm^{-1} (22%) usually assigned to b-turn and at 1613 cm^{-1} (27%), which could be assigned to side chains

460 vibrations; in contrast, mvG are mainly characterized by anti-parallel b-sheets structure (1632 (15%) and 1693 cm^{-1}

461 (3%) bands) with a strong contribution of flexible 3-10 helix (1661 cm^{-1} peak (34%)) and of side chain band at 1610

462 cm^{-1} (37%).

463

464   Finally, we set up a functional test to compare the impact of mvG delivery with that of mvA on

465 synaptic activity, when neuronal networks are acutely and transiently exposed to MVs. To this

466 aim, we isolated cortical neurons and glial cells from postnatal rat cortices and cultured them for

467 10 days. Fig. 4a shows confocal high magnification microscopy images of cortical cultures

468 where neurons were visualized by labeling class III β-tubulin (in red), a microtubule component

469 expressed exclusively by neurons, while astrocytes were visualized by GFAP labeling (in

470 green).[45] We patch-clamped visually identified cortical neurons (in voltage clamp

471 configuration, holding potential – 70 mV), while a second pipette for the local delivery of saline

472 solution was positioned at a distance of 200 μm (under microscopy visual control) from the

473 recorded cell (sketched in Fig. 4a, right). We estimated that, at this distance, the application of a

474 brief (500 ms) pulse of pressure should result in a local (i.e. on the recorded neuron) and

475 transient delivery of standard saline solution alone or containing mvG or mvA (re-suspended in

476 saline). A typical feature of these cultures is the prominent expression of spontaneous synaptic

477 activity, represented by heterogeneous postsynaptic currents (PSCs) of variable frequency and

478 amplitude (box plots in Fig. 4b). Baseline PSCs were recorded before (10 min) and after (15

479 min) the local saline, mvG or mvA ejection. Fig. 4c shows representative current tracings where

480 standard saline was pressure ejected (light grey, top), or where mvA solution (orange, middle)

481 and mvG (black, bottom) were administered.

482   Since spontaneous fluctuations in PSCs frequency ≤ 15 % of baseline values were frequently

483 detected, we took this as the threshold value to estimate changes when comparing PSCs before

484 and after pressure ejections of saline. In the large majority (88 %, n = 16/18 neurons; histograms

485 in Fig. 4d) of neurons exposed to saline solution alone, spontaneous PSCs frequency did not

486 change. On the contrary, within 5-8 min from the acute mvA and mvG ejections, PSCs frequency

487 was stably increased in 64 % (n= 16/25 neurons, mvA) and 54 % (n= 13/24 neurons, mvG;

488 summarized in the histograms of Fig. 4d) of recorded neurons. Fig. 4e shows the increases in

489 PSCs frequency in individual experiments and highlights the variability of such changes when

490 administering MVs, with increased frequencies ranging from 25 % to 200 %. Since we could not

491 experimentally control the amount of MVs collected by primary astrocytes and delivered by

492 pressure ejection, neurons were exposed to different amounts of MVs and this can in part explain

493 the detected variability. PSCs frequency increases due to MVs exposures were not reversible

494 upon 20 min washout. From such functional investigation, glial-signaling generated by ATP or s-

495 GO affected similarly neuronal synapses upon transient, direct exposure.

496   To our knowledge, this is the first time that the functional effects of MVs generated by

497 astrocytes on synaptic activity upon local delivery have been electrophysiologically documented.

498   Neuroglia extracellular vesicles have been described to provide support on synaptic activity, with

499   the majority of studies focused on microglia and inflammation, apparently regulating neural

500   transmission at the pre-synaptic level.[5,46–48] Astrocytic MVs have been proposed to exert

501   neuroprotective effects in neuropathology and in physiology, however the role of astrocytes or of

502   discrete astrocyte populations in delivering different messages via MV release has yet to be

503   elucidated.[49,50]

504   After assessment of the ability of MVs released by glial cells to affect cortical neuron

505   physiology within min after their interaction with the targeted neuron, we asked if the presumed

506   fusion of vesicles with neuronal plasma membrane could also affect their mechanical properties.

507   To investigate this aspect, we delivered MVs obtained from glial cultures previously treated with

508   bzATP or s-GO to cortical neurons by re-suspending the isolated MVs in 100 μL of neuronal

509   culture medium and adding them to neuronal cultures. 24 hours after the exposure, force

510   spectroscopy measurement on treated neuronal cultures were performed with AFM by

511   positioning the tipless cantilever with a borosilicate glass bead previously glued on it[51], at the

512   center of randomly chosen neurons. As showed by the boxplot in Fig. 4f, the exposure to mvA

513   caused a significant softening of neuronal soma, when compared to controls ($median_{mvA}$ = 0.22

514   kPa, $median_{control}$ = 0.59 kPa; P_{mvA} < 0.001). A similar result was observed also in the case of

515   mvG exposure even if the effect exerted on neuronal stiffness is less pronounced than that

516   induced by mvA ($median_{mvG}$ = 0.28 kPa, $median_{control}$ = 0.59 kPa; P_{mvG} < 0.01). The reported

517   effect of mvA and mvG on neuronal cell mechanical properties is presumably a consequence of

518   vesicular fusion with the cellular plasma membrane, which may affect its lipid composition.

519   Since the mechanical properties of a cell are mostly defined by plasma membrane features and

520   the ones of the underlying cytoskeleton, a change in neuronal plasma membrane lipid

26

521 composition can partially justify the observed reduction in mvA and mvG-treated neurons

522 stiffness.[52] In particular, glia-derived MVs are able to transport the enzyme Acid

523 sphingomyelinase (A-SMase) involved in the metabolism of sphingomyelin (SM), a precursor of

524 the phospholipid sphingosine (sph). Sph and its metabolites have been already reported to play a

525 fundamental role in facilitating synaptic vesicles release by changing the membrane composition

526 at pre-synaptic level.[48,53] This intrinsic capacity of MVs to participate in membrane lipid

527 metabolism may therefore modulate the contribution of plasma membrane to neuronal rigidity.

528 In this context, the slight difference of stiffness values reported among mvA and mvG-treated

529 neurons, although not statistically significant ($P_{mvA-mvG} > 0.05$) should not be

530 underestimated.[54,55] It is tempting to speculate that this difference can be explained by the

531 presence of specific proteins in the vesicles, that are unstable in mvG. Based on our measures,

532 we cannot exclude the presence of residual s-GO flakes either inside or on the vesicle surface. It

533 is known that GO is reportedly able to interact with the hydrophobic region of biological and

534 model lipid membranes, even though the nature of the interaction is strictly dependent to its size

535 and degree of surface oxygenation.[56,57] Assuming that the GO nanosheets, once added to the

536 culture medium, can adsorb on plasma membrane or pierce it and being embedded in the lipid

537 bilayer, there is a concrete possibility that MVs, which directly originate from plasma membrane,

538 can include those flakes in their structure.[30] The horizontal transfer of s-GO from glial cells to

539 cortical neurons, mediated by MVs, may therefore affect plasma membrane rigidity of targeted

540 neurons. Regardless of this, we can exclude a direct effect of s-GO in synaptic transmission,

541 reported to be transient and reversible upon acute exposure, in view of the persistent modulation

542 of synaptic current frequency brought about by MVs.[19,20]

a

b

c

d

e

f

g
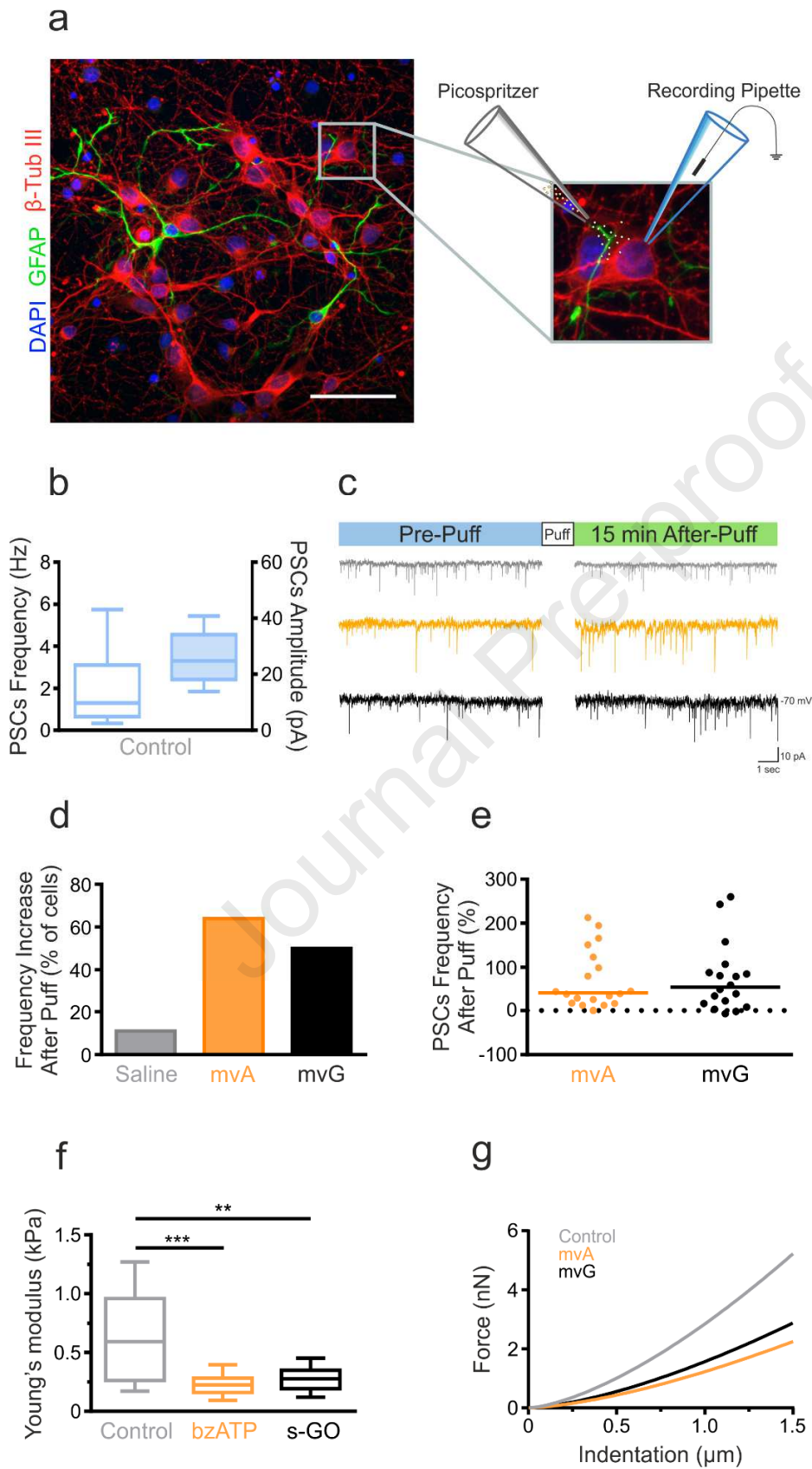
543

544 **Fig. 4. MVs released by astrocytes affect cortical neuron post-synaptic activity and mechanical properties.**
545 Potentiation of synaptic activity upon local applications of MVs in cortical neurons. a) Confocal micrograph
546 visualizing cortical primary cultures at 8 days in vitro; anti-class III β-tubulin is used to visualize neurons (in red),
547 anti-GFAP for astrocytes (in green) and DAPI (in blue) to visualize neurons. Scale bar 50 μm. On the right, a
548 representation of the experimental setting for the simultaneous MVs pressure-release (*puff*) and the cell patch-clamp
549 recording from cultured neurons. b) Box plot summarizes the PSCs frequency and amplitude values in control
550 cortical neurons. c) Top: diagram of the experimental protocol. Bottom: representative current tracings of the
551 spontaneous synaptic activity detected prior and after puff applications of control saline (in light grey) or mvA (in
552 orange) or mvG (in black). d) Bar plots of pooled data summarize the % of cells displaying PSCs frequency increase
553 upon delivery of pressure ejected saline (light grey), mvA (orange) and mvG (black). Note that in control (saline)
554 the large majority (88 %) of neurons did not increase their basal activity. e) The plot summarizes the distribution of
555 the % of increase in PCSs frequency detected within the three groups. f) Elastic moduli of cortical neurons, grown
556 on glass, and exposed to MVs isolated from glial cells previously treated with bzATP (orange) or s-GO flakes
557 (black). Neurons treated with mvA and mvG are significantly less rigid if compared with control ($P_{mvA} < 0.001$;
558 $P_{mvG} < 0.01$). Thick horizontal bars in the box plots indicate median value; boxed area extends from the 25th to 75th
559 percentiles, whiskers from 5th to the 95th percentiles. Significance: **$P < 0.01$ ***$P < 0.001$, Kruskal-Wallis test,
560 Dunn's post hoc test) **g.** Indentation curves of cortical neurons previously treated with mvA or mvG.

561

562 **4. Conclusion**

563 Astrocyte-derived MVs may play significant roles in propagating signaling molecules, in CNS

564 physiology and disease. Despite the increasing knowledge on extracellular vesicles (in particular

565 exosomes) ability to promote inflammation or contribute in spreading of pathogenic proteins in

566 neurodegenerative disorders (from Amyotrophic Lateral Sclerosis to Alzheimer disease [58,59])

567 little is currently known on their properties (mechanical, biochemical, lipid membrane

568 composition, cargo nature etc.), in particular when focusing on the smaller class of such natural

569 vectors, the MVs. Nevertheless, MVs emerge as key players in neuronal and synaptic

570 physiology, able to influence neurotransmission, or to support neurons.[48,60–62] In our study,

571 we report the ability of artificially generating MVs by s-GO transient exposure. MVs generated

572 by s-GO were apparently characterized by altered protein content when compared to the ATP-

573 driven ones. Intriguingly, the tuning of synaptic activity by mvG or mvA was similar,

574 supposedly being related to features diverse from MV protein content. The ability of s-GO to

575 interfere with exo-endocytotic membrane dynamics is not surprising, indeed we have described

576 the ability of s-GO nanoflakes to interfere with presynaptic vesicle release *in vitro* and *in*

577 *vivo*.[19,20] In the current work, we describe the direct interference of MVs with synaptic

578 activity, presumably due to MVs fusion with the target neuron plasma membrane. Such an

579 approach holds the potential to open new opportunities in engineering MVs for synaptic

580 targeting. In this framework, it is tempting to speculate that s-GO interactions with the cell

581 membrane mimic extracellular mechanical signaling at the nanoscale sufficient to enable the

582 release of MVs, thus representing unconventional tools to exploit the physics governing vesicle

583 release. We feel pertinent here to consider the fact, that the enormous potentiality of graphene-

584 based materials in nanomedicine has already promoted the development of new generation-

585 nanocarriers for either gene or drug delivery[17,63]. In this framework, we may speculate on

586 future developments where engineered cells are mechanically induced to release MVs, carrying

587 GO nanoflakes properly functionalized to deliver genes or drugs of interest and thus representing

588 either the trigger and the cargo.

589

590 ASSOCIATED CONTENT

591 **Supporting Information**

592   Supporting experimental section

593   Supporting results, Figures S1−S4 and Table S1.

594 AUTHOR INFORMATION

595 **Corresponding Author**

596   *E-mail: laura.ballerini@sissa.it

597   *E-mail: loredana.casalis@elettra.eu

598   **Present Addresses**

599   †Center for Synaptic Neuroscience, Istituto Italiano di Tecnologia (IIT), 16132, Genoa, Italy

600   **Author Contributions**

601   M.M. performed cell biology, electrophysiology, and immunofluorescence experiments and

602   analysis; M.M. and P.P. designed and performed AFM experiments; M.P. performed IR and

603   UVRR experiments and analysis. CM and GDM performed biology and WB experiments; N.L.

604   and K.K. contributed to the synthesis and characterization of thin graphene oxide of biological

605   grade. BB performed SEM micrographs of GO. L.B. and L.C. conceived the study; L.B.

606   conceived the experimental design and contributed to the analysis of data; L.B. wrote the

607   manuscript.

608   **Notes**

609   The authors declare no competing financial interest.

610

611   ACKNOWLEDGMENT

618 REFERENCES

619 [1] D.A. Shifrin, M.D. Beckler, R.J. Coffey, M.J. Tyska, Extracellular vesicles:

620   communication, coercion, and conditioning, Mol. Biol. Cell. 24 (2013) 1253–1259.

621   https://doi.org/10.1091/mbc.e12-08-0572.

622 [2] Y.J. Yoon, O.Y. Kim, Y.S. Gho, Extracellular vesicles as emerging intercellular

623   communicasomes., BMB Rep. 47 (2014) 531–9.

624   https://doi.org/10.5483/BMBREP.2014.47.10.164.

625 [3] V. Zappulli, K.P. Friis, Z. Fitzpatrick, C.A. Maguire, X.O. Breakefield, Extracellular

626   vesicles and intercellular communication within the nervous system, J. Clin. Invest. 126

627   (2016) 1198–1207. https://doi.org/10.1172/JCI81134.

628 [4] C.P.-K. Lai, X.O. Breakefield, Role of Exosomes/Microvesicles in the Nervous System

629   and Use in Emerging Therapies, Front. Physiol. 3 (2012) 228.

630   https://doi.org/10.3389/fphys.2012.00228.

631 [5] V. Budnik, C. Ruiz-Cañada, F. Wendler, Extracellular vesicles round off communication

632   in the nervous system., Nat. Rev. Neurosci. 17 (2016) 160–72.

633   https://doi.org/10.1038/nrn.2015.29.

634 [6] A. Grimaldi, C. Serpe, G. Chece, V. Nigro, A. Sarra, B. Ruzicka, M. Relucenti, G.

635   Familiari, G. Ruocco, G.R. Pascucci, F. Guerrieri, C. Limatola, M. Catalano, Microglia-

636   Derived Microvesicles Affect Microglia Phenotype in Glioma, Front. Cell. Neurosci. 13

637   (2019) 41. https://doi.org/10.3389/fncel.2019.00041.

638   [7]   E. Cocucci, J. Meldolesi, Ectosomes and exosomes: shedding the confusion between

639   extracellular vesicles., Trends Cell Biol. 25 (2015) 364–72.

640   https://doi.org/10.1016/j.tcb.2015.01.004.

641   [8]   G. Raposo, W. Stoorvogel, Extracellular vesicles: exosomes, microvesicles, and friends.,

642   J. Cell Biol. 200 (2013) 373–83. https://doi.org/10.1083/jcb.201211138.

643   [9]   S.L.N. Maas, X.O. Breakefield, A.M. Weaver, Extracellular Vesicles: Unique Intercellular

644   Delivery Vehicles, Trends Cell Biol. 27 (2017) 172–188.

645   https://doi.org/10.1016/j.tcb.2016.11.003.

646   [10] C. Frühbeis, D. Fröhlich, E.-M. Krämer-Albers, Emerging Roles of Exosomes in Neuron–

647   Glia Communication, Front. Physiol. 3 (2012) 119.

648   https://doi.org/10.3389/fphys.2012.00119.

649   [11] G. Lachenal, K. Pernet-Gallay, M. Chivet, F.J. Hemming, A. Belly, G. Bodon, B. Blot, G.

650   Haase, Y. Goldberg, R. Sadoul, Release of exosomes from differentiated neurons and its

651   regulation by synaptic glutamatergic activity., Mol. Cell. Neurosci. 46 (2011) 409–18.

652   https://doi.org/10.1016/j.mcn.2010.11.004.

653   [12] K.E. van der Vos, L. Balaj, J. Skog, X.O. Breakefield, Brain tumor microvesicles: insights

654   into intercellular communication in the nervous system., Cell. Mol. Neurobiol. 31 (2011)

655   949–59. https://doi.org/10.1007/s10571-011-9697-y.

656   [13] D. Ha, N. Yang, V. Nadithe, Exosomes as therapeutic drug carriers and delivery vehicles

657   across biological membranes: current perspectives and future challenges, Acta Pharm. Sin.

658   B. 6 (2016) 287–296. https://doi.org/10.1016/J.APSB.2016.02.001.

659 [14] C. Verderio, L. Muzio, E. Turola, A. Bergami, L. Novellino, F. Ruffini, L. Riganti, I.

660   Corradini, M. Francolini, L. Garzetti, C. Maiorino, F. Servida, A. Vercelli, M. Rocca,

661   D.D. Libera, V. Martinelli, G. Comi, G. Martino, M. Matteoli, R. Furlan, Myeloid

662   microvesicles are a marker and therapeutic target for neuroinflammation, Ann. Neurol. 72

663   (2012) 610–624. https://doi.org/10.1002/ana.23627.

664 [15] S. EL Andaloussi, I. Mäger, X.O. Breakefield, M.J.A. Wood, Extracellular vesicles:

665   biology and emerging therapeutic opportunities, Nat. Rev. Drug Discov. 12 (2013) 347–

666   357. https://doi.org/10.1038/nrd3978.

667 [16] K.P. Loh, Q. Bao, G. Eda, M. Chhowalla, Graphene oxide as a chemically tunable

668   platform for optical applications, Nat. Chem. 2 (2010) 1015–1024.

669   https://doi.org/10.1038/nchem.907.

670 [17] G. Reina, J.M. González-Domínguez, A. Criado, E. Vázquez, A. Bianco, M. Prato,

671   Promises, facts and challenges for graphene in biomedical applications, Chem. Soc. Rev.

672   46 (2017) 4400–4416. https://doi.org/10.1039/c7cs00363c.

673 [18] M. Baldrighi, M. Trusel, R. Tonini, S. Giordani, Carbon Nanomaterials Interfacing with

674   Neurons: An In vivo Perspective, Front. Neurosci. 10 (2016) 250.

675   https://doi.org/10.3389/fnins.2016.00250.

676 [19] R. Rauti, N. Lozano, V. León, D. Scaini, M. Musto, I. Rago, F.P. Ulloa Severino, A.

677   Fabbro, L. Casalis, E. Vázquez, K. Kostarelos, M. Prato, L. Ballerini, Graphene Oxide

678   Nanosheets Reshape Synaptic Function in Cultured Brain Networks, ACS Nano. 10

679   (2016) 4459–4471. https://doi.org/10.1021/acsnano.6b00130.

680   [20]   R. Rauti, M. Medelin, L. Newman, S. Vranic, G. Reina, A. Bianco, M. Prato, K.

681   Kostarelos, L. Ballerini, Graphene Oxide Flakes Tune Excitatory Neurotransmission in

682   Vivo by Targeting Hippocampal Synapses, Nano Lett. 19 (2019) 2858–2870.

683   https://doi.org/10.1021/acs.nanolett.8b04903.

684   [21]   Z. Song, Y. Wang, Z. Xu, Mechanical responses of the bio-nano interface: A molecular

685   dynamics study of graphene-coated lipid membrane, Theor. Appl. Mech. Lett. 5 (2015)

686   231–235. https://doi.org/10.1016/j.taml.2015.11.003.

687   [22]   R.J. Rodrigues, A.R. Tomé, R.A. Cunha, ATP as a multi-target danger signal in the brain,

688   Front. Neurosci. 9 (2015) 148. https://doi.org/10.3389/fnins.2015.00148.

689   [23]   F. Calegari, S. Coco, E. Taverna, M. Bassetti, C. Verderio, N. Corradi, M. Matteoli, P.

690   Rosa, A regulated secretory pathway in cultured hippocampal astrocytes., J. Biol. Chem.

691   274 (1999) 22539–47.

692   [24]   P. Hermanowicz, M. Sarna, K. Burda, H. Gabryś, AtomicJ: An open source software for

693   analysis of force curves, Rev. Sci. Instrum. 85 (2014) 063703.

694   https://doi.org/10.1063/1.4881683.

695   [25]   F. D'Amico, M. Saito, F. Bencivenga, M. Marsi, A. Gessini, G. Camisasca, E. Principi, R.

696   Cucini, S. Di Fonzo, A. Battistoni, E. Giangrisostomi, C. Masciovecchio, UV resonant

697   Raman scattering facility at Elettra, Nucl. Instruments Methods Phys. Res. Sect. A Accel.

698   Spectrometers, Detect. Assoc. Equip. 703 (2013) 33–37.

699   https://doi.org/10.1016/J.NIMA.2012.11.037.

700 [26] A. Bignami, L.F. Eng, D. Dahl, C.T. Uyeda, Localization of the glial fibrillary acidic

701 protein in astrocytes by immunofluorescence, Brain Res. 43 (1972) 429–435.

702 https://doi.org/10.1016/0006-8993(72)90398-8.

703 [27] M. Musto, R. Rauti, A.F. Rodrigues, E. Bonechi, C. Ballerini, K. Kostarelos, L. Ballerini,

704 3D Organotypic Spinal Cultures: Exploring Neuron and Neuroglia Responses Upon

705 Prolonged Exposure to Graphene Oxide, Front. Syst. Neurosci. 13 (2019) 1.

706 https://doi.org/10.3389/fnsys.2019.00001.

707 [28] M. Bramini, G. Alberini, E. Colombo, M. Chiacchiaretta, M.L. DiFrancesco, J.F. Maya-

708 Vetencourt, L. Maragliano, F. Benfenati, F. Cesca, Interfacing graphene-based materials

709 with neural cells, Front. Syst. Neurosci. 12 (2018) 12.

710 https://doi.org/10.3389/fnsys.2018.00012.

711 [29] A.B. Seabra, A.J. Paula, R. De Lima, O.L. Alves, N. Durán, Nanotoxicity of graphene and

712 graphene oxide, Chem. Res. Toxicol. 27 (2014) 159–168.

713 https://doi.org/10.1021/tx400385x.

714 [30] F. Bianco, C. Perrotta, L. Novellino, M. Francolini, L. Riganti, E. Menna, L. Saglietti,

715 E.H. Schuchman, R. Furlan, E. Clementi, M. Matteoli, C. Verderio, Acid

716 sphingomyelinase activity triggers microparticle release from glial cells, EMBO J. 28

717 (2009) 1043–1054. https://doi.org/10.1038/emboj.2009.45.

718 [31] E. Amaral, S. Guatimosim, C. Guatimosim, Using the Fluorescent Styryl Dye FM1-43 to

719 Visualize Synaptic Vesicles Exocytosis and Endocytosis in Motor Nerve Terminals, in:

720 Methods Mol. Biol., 2011: pp. 137–148. https://doi.org/10.1007/978-1-60761-950-5_8.

721   [32] W.J. Betz, F. Mao, C.B. Smith, Imaging exocytosis and endocytosis, Curr. Opin.

722   Neurobiol. 6 (1996) 365–371. https://doi.org/10.1016/S0959-4388(96)80121-8.

723   [33] A. Brumback, J.L. Lieber, J.K. Angleson, W.J. Betz, Using FM1-43 to study neuropeptide

724   granule   dynamics   and   exocytosis,   Methods.   33   (2004)   287–294.

725   https://doi.org/10.1016/j.ymeth.2004.01.002.

726   [34] Y. Yoshioka, Y. Konishi, N. Kosaka, T. Katsuda, T. Kato, T. Ochiya, Comparative

727   marker analysis of extracellular vesicles in different human cancer types., J. Extracell.

728   Vesicles. 2 (2013). https://doi.org/10.3402/jev.v2i0.20424.

729   [35] R.A. Dragovic, C. Gardiner, A.S. Brooks, D.S. Tannetta, D.J.P. Ferguson, P. Hole, B.

730   Carr, C.W.G. Redman, A.L. Harris, P.J. Dobson, P. Harrison, I.L. Sargent, Sizing and

731   phenotyping of cellular vesicles using Nanoparticle Tracking Analysis., Nanomedicine. 7

732   (2011) 780–8. https://doi.org/10.1016/j.nano.2011.04.003.

733   [36] T. Visnovitz, X. Osteikoetxea, B.W. Sódar, J. Mihály, P. Lőrincz, K. V. Vukman, E.Á.

734   Tóth, A. Koncz, I. Székács, R. Horváth, Z. Varga, E.I. Buzás, An improved 96 well plate

735   format lipid quantification assay for standardisation of experiments with extracellular

736   vesicles,   J.   Extracell.   Vesicles.   8   (2019)   1565263.

737   https://doi.org/10.1080/20013078.2019.1565263.

738   [37] J. Mihály, R. Deák, I.C. Szigyártó, A. Bóta, T. Beke-Somfai, Z. Varga, Characterization

739   of extracellular vesicles by IR spectroscopy: Fast and simple classification based on amide

740   and C H stretching vibrations, Biochim. Biophys. Acta - Biomembr. 1859 (2017) 459–

741   466. https://doi.org/10.1016/j.bbamem.2016.12.005.

742   [38]   D. Ami, F. Lavatelli, P. Rognoni, G. Palladini, S. Raimondi, S. Giorgetti, L. Monti, S.M.

743   Doglia, A. Natalello, G. Merlini, In situ characterization of protein aggregates in human

744   tissues affected by light chain amyloidosis: a FTIR microspectroscopy study, Sci. Rep. 6

745   (2016) 29096. https://doi.org/10.1038/srep29096.

746   [39]   A. Németh, N. Orgovan, B.W. Sódar, X. Osteikoetxea, K. Pálóczi, K. Szabó-Taylor, K. V.

747   Vukman, Á. Kittel, L. Turiák, Z. Wiener, S. Tóth, L. Drahos, K. Vékey, R. Horvath, E.I.

748   Buzás, Antibiotic-induced release of small extracellular vesicles (exosomes) with surface-

749   associated DNA, Sci. Rep. 7 (2017) 1–16. https://doi.org/10.1038/s41598-017-08392-1.

750   [40]   M.Y. Sherman, A.L. Goldberg, Cellular defenses against unfolded proteins: a cell

751   biologist thinks about neurodegenerative diseases., Neuron. 29 (2001) 15–32.

752   https://doi.org/10.1016/s0896-6273(01)00177-5.

753   [41]   R. V Rao, D.E. Bredesen, Misfolded proteins, endoplasmic reticulum stress and

754   neurodegeneration., Curr. Opin. Cell Biol. 16 (2004) 653–62.

755   https://doi.org/10.1016/j.ceb.2004.09.012.

756   [42]   D.J. Selkoe, Folding proteins in fatal ways, Nature. 426 (2003) 900–904.

757   https://doi.org/10.1038/nature02264.

758   [43]   A. Natalello, D. Ami, S.M. Doglia, Fourier Transform Infrared Spectroscopy of

759   Intrinsically Disordered Proteins: Measurement Procedures and Data Analyses, in:

760   Methods Mol. Biol., 2012: pp. 229–244. https://doi.org/10.1007/978-1-61779-927-3_16.

761   [44]   C.J. Oldfield, A.K. Dunker, Intrinsically Disordered Proteins and Intrinsically Disordered

762   Protein Regions, Annu. Rev. Biochem. 83 (2014) 553–584.

763   https://doi.org/10.1146/annurev-biochem-072711-164947.

764   [45] D. V Caccamo, M.M. Herman, A. Frankfurter, C.D. Katsetos, V.P. Collins, L.J.

765   Rubinstein, An immunohistochemical study of neuropeptides and neuronal cytoskeletal

766   proteins in the neuroepithelial component of a spontaneous murine ovarian teratoma.

767   Primitive neuroepithelium displays immunoreactivity for neuropeptides and neuron-

768   associated beta-tu, Am. J. Pathol. 135 (1989) 801–13.

769   [46] R.C. Paolicelli, G. Bergamini, L. Rajendran, Cell-to-cell Communication by Extracellular

770   Vesicles: Focus   on   Microglia,   Neuroscience.   (2018).

771   https://doi.org/10.1016/j.neuroscience.2018.04.003.

772   [47] Y. Yang, A. Boza-Serrano, C.J.R. Dunning, B.H. Clausen, K.L. Lambertsen, T.

773   Deierborg, Inflammation leads to distinct populations of extracellular vesicles from

774   microglia, J. Neuroinflammation. 15 (2018) 168. https://doi.org/10.1186/s12974-018-

775   1204-7.

776   [48] F. Antonucci, E. Turola, L. Riganti, M. Caleo, M. Gabrielli, C. Perrotta, L. Novellino, E.

777   Clementi, P. Giussani, P. Viani, M. Matteoli, C. Verderio, Microvesicles released from

778   microglia stimulate synaptic activity via enhanced sphingolipid metabolism, EMBO J. 31

779   (2012) 1231–1240. https://doi.org/10.1038/emboj.2011.489.

780   [49] M.J. Carson, J.C. Thrash, B. Walter, The cellular response in neuroinflammation: The role

781   of leukocytes, microglia and astrocytes in neuronal death and survival., Clin. Neurosci.

782   Res. 6 (2006) 237–245. https://doi.org/10.1016/j.cnr.2006.09.004.

783   [50] M.M. Holm, J. Kaiser, M.E. Schwab, Extracellular Vesicles: Multimodal Envoys in

784   Neural Maintenance and Repair., Trends Neurosci. 41 (2018) 360–372.

785   https://doi.org/10.1016/j.tins.2018.03.006.

786   [51] T. Gerecsei, I. Erdődi, B. Peter, C. Hős, S. Kurunczi, I. Derényi, B. Szabó, R. Horvath,

787   Adhesion force measurements on functionalized microbeads: An in-depth comparison of

788   computer controlled micropipette and fluidic force microscopy, J. Colloid Interface Sci.

789   555 (2019) 245–253. https://doi.org/10.1016/j.jcis.2019.07.102.

790   [52] S. Kasas, X. Wang, H. Hirling, R. Marsault, B. Huni, A. Yersin, R. Regazzi, G.

791   Grenningloh, B. Riederer, L. Forrò, G. Dietler, S. Catsicas, Superficial and deep changes

792   of cellular mechanical properties following cytoskeleton disassembly, Cell Motil.

793   Cytoskeleton. 62 (2005) 124–132. https://doi.org/10.1002/cm.20086.

794   [53] E. Norman, R.G. Cutler, R. Flannery, Y. Wang, M.P. Mattson, Plasma membrane

795   sphingomyelin hydrolysis increases hippocampal neuron excitability by sphingosine-1-

796   phosphate mediated mechanisms, J. Neurochem. 114 (2010) 430–439.

797   https://doi.org/10.1111/j.1471-4159.2010.06779.x.

798   [54] V. Amrhein, S. Greenland, B. McShane, Scientists rise up against statistical significance,

799   Nature. 567 (2019) 305–307. https://doi.org/10.1038/d41586-019-00857-9.

800   [55] It's time to talk about ditching statistical significance, Nature. 567 (2019) 283–283.

801   https://doi.org/10.1038/d41586-019-00874-8.

802   [56] R. Frost, S. Svedhem, C. Langhammer, B. Kasemo, Graphene Oxide and Lipid

803   Membranes: Size-Dependent Interactions, Langmuir. 32 (2016) 2708–2717.

804   https://doi.org/10.1021/acs.langmuir.5b03239.

805   [57]   N. Li, Q. Zhang, S. Gao, Q. Song, R. Huang, L. Wang, L. Liu, J. Dai, M. Tang, G. Cheng,

806   Three-dimensional graphene foam as a biocompatible and conductive scaffold for neural

807   stem cells, Sci. Rep. 3 (2013) 1604. https://doi.org/10.1038/srep01604.

808   [58]   M. Basso, S. Pozzi, M. Tortarolo, F. Fiordaliso, C. Bisighini, L. Pasetto, G. Spaltro, D.

809   Lidonnici, F. Gensano, E. Battaglia, C. Bendotti, V. Bonetto, Mutant copper-zinc

810   superoxide dismutase (SOD1) induces protein secretion pathway alterations and exosome

811   release in astrocytes: implications for disease spreading and motor neuron pathology in

812   amyotrophic   lateral   sclerosis.,   J.   Biol.   Chem.   288   (2013)   15699–711.

813   https://doi.org/10.1074/jbc.M112.425066.

814   [59]   G. Wang, M. Dinkins, Q. He, G. Zhu, C. Poirier, A. Campbell, M. Mayer-Proschel, E.

815   Bieberich, Astrocytes Secrete Exosomes Enriched with Proapoptotic Ceramide and

816   Prostate Apoptosis Response 4 (PAR-4), J. Biol. Chem. 287 (2012) 21384–21395.

817   https://doi.org/10.1074/jbc.M112.340513.

818   [60]   R.-D. Gosselin, P. Meylan, I. Decosterd, Extracellular microvesicles from astrocytes

819   contain functional glutamate transporters: regulation by protein kinase C and cell

820   activation., Front. Cell. Neurosci. 7 (2013) 251. https://doi.org/10.3389/fncel.2013.00251.

821   [61]   A.R. Taylor, M.B. Robinson, D.J. Gifondorwa, M. Tytell, C.E. Milligan, Regulation of

822   heat shock protein 70 release in astrocytes: Role of signaling kinases, Dev. Neurobiol. 67

823   (2007) 1815–1829. https://doi.org/10.1002/dneu.20559.

824   [62]   S. Wang, F. Cesca, G. Loers, M. Schweizer, F. Buck, F. Benfenati, M. Schachner, R.

825   Kleene, Synapsin I Is an Oligomannose-Carrying Glycoprotein, Acts As an

826   Oligomannose-Binding Lectin, and Promotes Neurite Outgrowth and Neuronal Survival

827   When Released via Glia-Derived Exosomes, J. Neurosci. 31 (2011) 7275–7290.

828   https://doi.org/10.1523/JNEUROSCI.6476-10.2011.

829   [63] H. Zhao, R. Ding, X. Zhao, Y. Li, L. Qu, H. Pei, L. Yildirimer, Z. Wu, W. Zhang,

830   Graphene-based nanomaterials for drug and/or gene delivery, bioimaging, and tissue

831   engineering, Drug Discov. Today. 22 (2017) 1302–1317.

832   https://doi.org/10.1016/j.drudis.2017.04.002.

HIGHLIGHTS

Graphene oxide interferes with cell membrane dynamics and enhance astrocytes' release of MVs

MVs driven by graphene oxide stimuli display a different protein profile from chemically driven ones

MVs released upon graphene oxide exposure affect neuronal signaling and membrane stiffness

Shedding Plasma Membrane Vesicles Induced by Graphene Oxide Nanoflakes in Brain Cultured Astrocytes

Mattia Musto[1†], Pietro Parisse[2], Maria Pachetti[2], Christian Memo[1], Giuseppe Di Mauro[1], Belen Ballesteros[3], Neus Lozano[3], Kostas Kostarelos[3,4], Loredana Casalis[2*] and Laura Ballerini[1*]

[1]International School for Advanced Studies (SISSA), 34136 Trieste, Italy
[2]ELETTRA Synchrotron Light Source, 34149 Basovizza, Italy
[3]Catalan Institute of Nanoscience and Nanotechnology (ICN2), Campus UAB, Bellaterra, 08193 Barcelona, Spain
[4]Nanomedicine Lab, National Graphene Institute and Faculty of Biology, Medicine & Health The University of Manchester, Manchester M13 9PT, United Kingdom

Conflict of interest

Authors declare no competing interests.